Plasma Sources Sci. Technol. **21** (2012) 055003 (7pp) doi:10.1088/0963-0252/21/5/055003

Laser wavelength dependence on angular emission dynamics of Nd : YAG laser-produced Sn plasmas

J R Freeman[1], S S Harilal[1], B Verhoff[1], A Hassanein[1] and B Rice[2]

[1] Center for Materials Under Extreme Environment, School of Nuclear Engineering, Purdue University, West Lafayette, IN 47907, USA
[2] SEMATECH Inc. Albany, NY 12203, USA

E-mail: freemaj@purdue.edu

Received 7 May 2012, in final form 9 July 2012
Published 10 August 2012
Online at stacks.iop.org/PSST/21/055003

Abstract
We investigated the laser wavelength effect on angular atomic and ionic emission from laser-produced Sn plasma, since it is regarded as a viable candidate for an EUV lithography source. For producing plasmas, the fundamental, second and fourth harmonics radiation from a Nd : YAG laser were used. The angular variation of atomic and ionic particle analysis was carried out using quartz crystal microbalance and Faraday cups by moving them in a circular path at a constant distance from the target normal. Along with atomic and ionic emission, we also compared the plasma emission features in the visible and EUV spectral regions. Results indicate strong forward bias in atomic and ionic plasma debris at all wavelengths. Shorter wavelength plasmas are found to generate more atomic particles while ion flux showed a similar trend irrespective of the excitation wavelength.

(Some figures may appear in colour only in the online journal)

1. Introduction

Laser-produced plasmas (LPPs) are routinely used for numerous applications. Some of the prominent applications are light sources for lithography and microscopy [1], laser-induced breakdown spectroscopy (LIBS) [2], pulsed laser deposition (PLD) [3], nanocluster and nanotube production [4], sample introduction in inductively coupled-plasma mass spectrometry (ICP-MS) [5], etc. Basic understanding of plasma emission, expansion, and kinetic properties of the ejected particles from the plasma is essential for optimization in all applications of LPPs. The properties of LPPs depend strongly on both target as well as laser properties. Among the laser parameters, wavelength and pulse width of the pumping laser play a major role in laser–target and laser–plasma coupling and they are directly connected to all properties of the produced plasma (e.g. absorption, mass ablation, emission, opacity, etc).

Currently, significant effort is being devoted to developing debris-free and efficient Sn plasma light sources at 13.5 nm for the next-generation extreme ultraviolet lithography (EUVL). Studies have shown that both Nd : YAG and CO_2 lasers [6, 7] are viable LPP drivers, owing to high conversion efficiencies (CEs). However, the CO_2 LPP provides higher CE and less debris compared to 1064 nm LPP [8, 9]. Debris in EUVL LPP light sources includes energetic atoms and ions, out-of-band (OoB) emission, etc. In an EUVL system, debris accumulation on the collector optics is still a major issue, and therefore source optimization cannot be considered complete without efficient debris mitigation systems [10, 11]. Debris mitigation of both ions and atoms is imperative for preserving mirror lifetime. The accumulation of debris on the mirror not only drives down EUV reflectivity, but highly energetic species can cause sputtering and interlayer mixing of mirror constituents. Moreover, the near 70% reflection of in-band radiation typically demonstrated by industrially standard Mo/Si optics means that 30% of the in-band radiation can be absorbed by the mirror, in addition to OoB emission [12]. Heat loading on the mirror can be significant, which can cause surface warping and also degrade reflectivity [13]. Hence, a comprehensive study to understand the debris generation of Nd : YAG LPPs is desirable. In this paper we show the laser wavelength and angular dependence of the debris generated by a Nd : YAG LPP EUV source. The

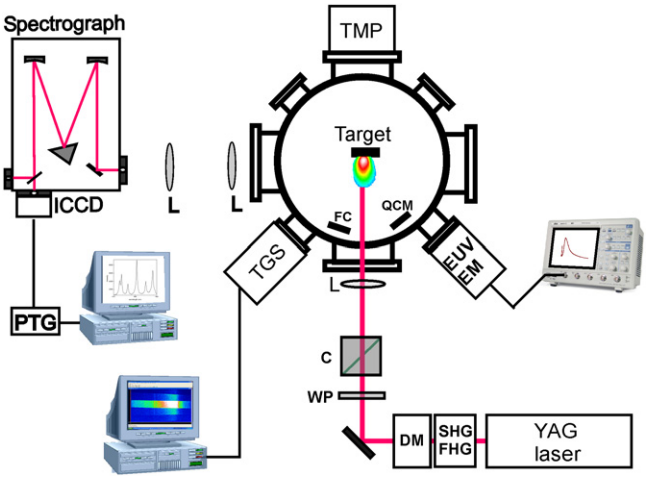

Figure 1. The schematic of the experimental set up: (SHG, second harmonic generator; FHG, fourth harmonic generator; DM, dichroic mirrors; WP, waveplate; C, polarizing cube; L, lens; QCM, quartz crystal microbalance; FC, Faraday cup; ICCD, intensified charge-coupled device; PTG, programmable timing generator; TMP, turbomolecular pump; EUV EM, EUV energy monitor; TGS, transmission grating spectrograph).

diagnostic tools used in the present investigation include EUV and optical emission spectroscopy, quartz crystal microbalance (QCM), and ionic debris characterization via a Faraday cup (FC). Our recent results have shown that CO_2-produced laser plasmas emit less debris compared to Nd : YAG LPP at fundamental wavelengths [11, 14]. This study further investigates the emission from Nd : YAG laser-produced tin plasmas, specifically focusing on the changes in debris generation as a function of laser wavelength (Nd : YAG fundamental wavelength and harmonics). In particular, a pronounced forward bias is shown for the Nd : YAG LPP atomic and ionic debris at fundamental, second and fourth harmonics, where debris generation decreases significantly at high off-normal target angles. It is further demonstrated that high off-normal target angles generate similarly low amounts of debris regardless of the incident wavelength.

2. Experimental setup

The schematic of the experimental setup is shown in figure 1. For creating the plasma, pulses from the Nd : YAG laser were used. The full-width half-maximum (FWHM) of the 1064 nm radiation was 6 ns. The fundamental radiation (ω) was frequency doubled (2ω) and quadrupled (4ω) using KDP crystals, and dichroic mirrors were used for frequency separation. The laser radiation was focused onto a planar tin target in vacuum (base pressure $\sim 10^{-5}$ Torr) mounted on a servo-motor controlled *XYZ* translation stage granting micrometer precision in three dimensions. The spot size at the target was measured to be $100 \pm 10\,\mu$m and the laser was incident normal to the target surface. At each wavelength, the focusing lens was repositioned to retain the same spot size.

For the optical emission studies, we employed a 0.5 m spectrograph equipped with an intensified charge-coupled device (ICCD) to characterize the plasma emission in the visible range. The wavelength dispersed spectra were obtained using a 150 grooves mm^{-1} grating. We performed the emission spectroscopic studies and imaging analyses at a position normal to the direction of plasma expansion. A programmable timing generator was used for synchronizing the laser with ICCD. For obtaining the visible spectrum of the plasmas, we set the ICCD gate to start 100 ns after the onset of the laser pulse and to be exposed to the plasma emission for 3 μs. For the EUV spectroscopic studies, a spectrograph equipped with a transmission grating (10 000 grooves mm^{-1}) is employed and the dispersed spectra are recorded using a time-gated EUV sensitive camera.

Ionic analysis was performed with a Kimball Physics FC on a rotatable manipulator placed at 14 cm from the Sn target and biased to -31 V to screen electrons. The manipulator allowed the FC to be rotated through off-normal target angles between 15° and 65°. The FC was paired with a photo-detector and an oscilloscope for data analysis. For atomic analysis, a QCM was used, also on a rotatable manipulator. The QCM consists of a silver crystal microbalance sensor attached to an Inficon XTM-2 deposition monitor.

3. Results

The optimum CE for EUV generation is a function of power density and spot size [8, 15]. The Nd : YAG fundamental wavelength optimum conditions are 1.5×10^{11} W cm^{-2} at 100 μm spot size that provided 2% CE [16]. We used this same power density ($(1.5 \pm 0.2) \times 10^{11}$ W cm^{-2}) for ω, 2ω and 4ω for obtaining a reasonable comparison of the debris from the YAG LPP. It should be mentioned that among the wavelengths studied, the 1064 nm provided the highest CE [17]. However, along with higher CE, minimum plasma debris is also one of the utmost considerations for EUVL source. We made a systematic comparison of EUV and visible emission features of plasmas generated by Nd : YAG fundamental and harmonics along with angular features of atomic and ionic particle emission.

3.1. EUV and visible spectra characterization

To examine the underlying mechanisms causing disparities in the debris emission, we performed detailed spectroscopic studies of the plasmas. Spectroscopic studies provide better understanding of radiative emission from the plasma and thus OoB heat loading to the collector optics of a lithography system. The recorded normalized Sn unresolved transition array (UTA) for ω, 2ω and 4ω produced plasmas are given in figure 2 along with a CO_2 LPP spectrum for comparison. The UTA emission is concentrated around 13.5 nm, with a narrow band gap of 5–10 eV arising from the $4p^6 4d^n - 4p^5 4d^{n+1} + 4p^6 4d^{n-1} 4f$ transitions of various Sn ions, ranging from Sn^{6+} to Sn^{14+}, with occupancy in transition levels from the range of $n = 2$ to $n = 8$. The main contributors of emission in the in-band region are Sn^{9+}–Sn^{13+} ions and lower ionic states mainly contribute to the emission in the higher wavelength region of the UTA. The recorded spectra showed highest and lowest in-band intensities for ω and 4ω, respectively, which

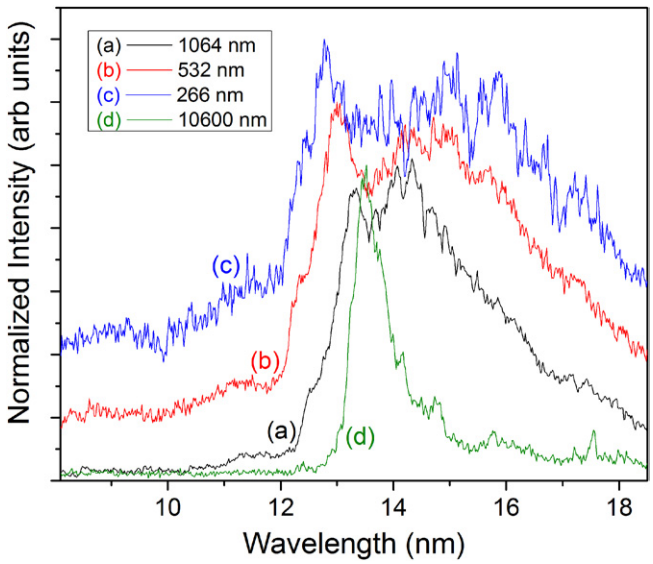

Figure 2. Normalized EUV emission spectra for the ω, 2ω, and 4ω Nd : YAG LPP and 10.6 μm CO_2 LPP for reference. The power density at the target was 1.5×10^{11} W cm^{-2} for generating the Nd : YAG LPP. The 2ω, and 4ω spectra are scaled upward for a better view.

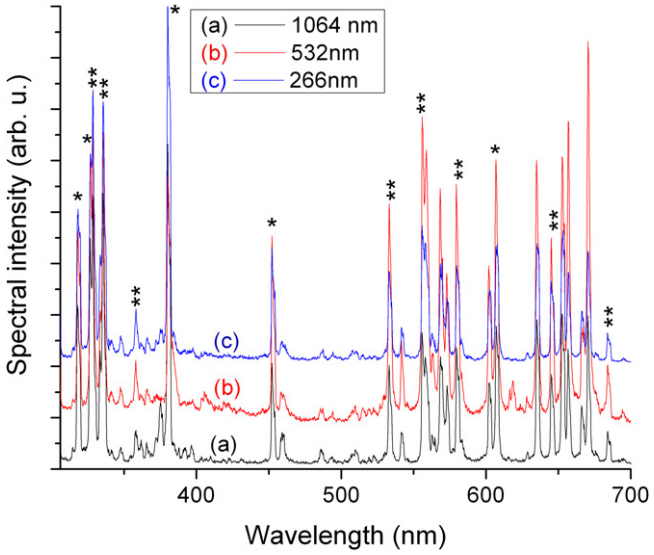

Figure 3. Visible emission spectra of the ω, 2ω and 4ω YAG LPP taken at 1 mm from the target. The *labeled peaks are emission from neutral tin and the **labeled peaks are emission from Sn^+. The unlabeled peaked are due to second order diffraction from the grating. The spectra are shifted upward for a better view.

is consistent with reported EUV spectra [18]. Immediately evident from the emission spectra is the considerably broader UTA arising from all harmonics of YAG laser compared to UTA emission from CO_2 LPP [8]. In order to achieve similar plasma temperature and EUV emission, laser power density for the Nd : YAG LPP must be greater than that for the CO_2 LPP due to two order higher critical density of the Nd : YAG LPP [19]. The Nd : YAG LPPs emits a considerable amount of OoB emission on the longer wavelength side of the UTA due to increased populations of lower ionic states. Moreover, self-absorption is evident in UTAs recorded from Nd : YAG produced plasmas irrespective of the excitation wavelength used.

We extended OoB emission studies to visible emission region by recording the spectra of the LPP produced by various harmonics of the YAG laser. The spectral emission from the plasma was collected using an optical system and imaged onto the slit of a spectrograph. We manipulated the optics such that the image of the target was 1 mm away from the spectrograph slit. These emission spectra were time-integrated over 3 μs starting from a delay of 100 ns with respect to the incident laser pulses. The purpose of delaying the ICCD gate by 100 ns is to avoid intense continuum emission during the earliest time of plasma evolution. Figure 3 shows the visible emission of Sn plasma from the ω, 2ω and 4ω YAG LPP. The identified lines from the literature [20] are marked in the figure. The unmarked lines are due to second order diffracted lines. Most of the identified lines are due to neutral or singly ionized Sn. Our previous results showed that CO_2 LPP contains stronger ionic peaks compared to the Nd : YAG LPP [21]. In the case of the denser, shorter wavelength Nd : YAG plasmas, the extended recombination zone results in the production of lower charged ions and neutral debris farther away from the target. Unlike EUV spectral features, there was no discernible difference between the ω, 2ω and 4ω YAG LPP spectra under same laser irradiance conditions.

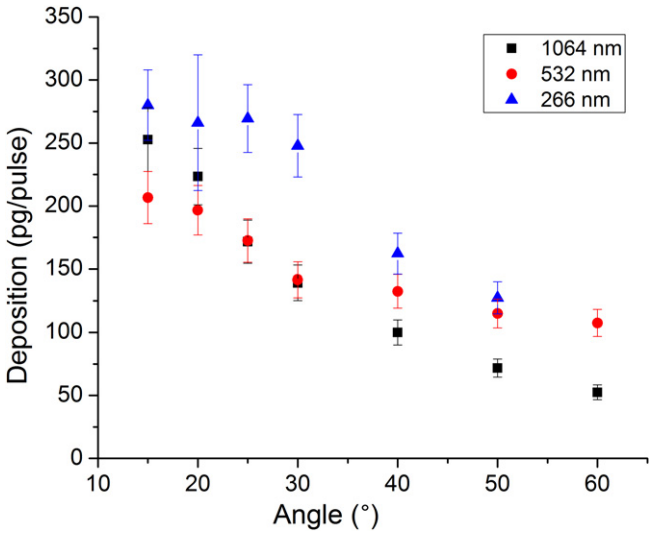

Figure 4. Angular variation of deposited mass estimated using a QCM. For this analysis QCM was placed 14 cm from the target. Each experimental data point is obtained from averaging 500 laser shots. Error bars indicate the standard deviation of several averaged data points at each angle.

3.2. Atomic debris studies

In addition to photon emission, characterization of atomic debris emission was performed using a QCM. Atomic debris studies are critical for understanding their effect on mirror reflectivity degradation. For angular studies, the QCM is fixed on a precisely calibrated rotatable manipulator that allows for placement accuracy within one degree. For the purposes of this study, it was rotated on 5° intervals between 15° and 65°. Figure 4 shows the angular variation of deposited mass on the

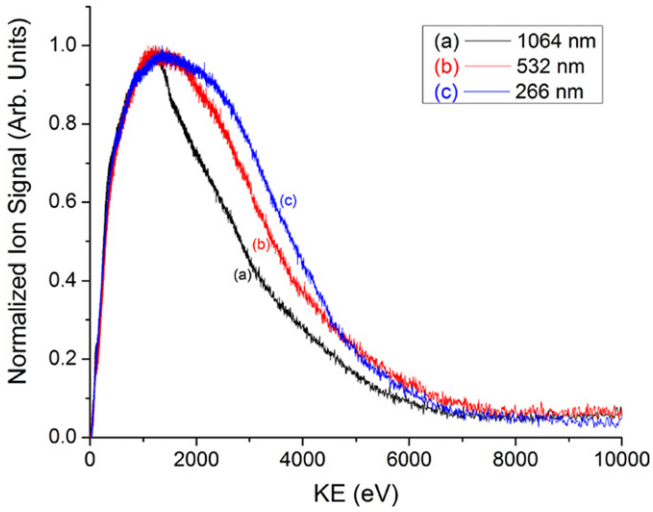

Figure 5. Kinetic energy distribution of ions from the Sn LPP generated by various wavelengths of the Nd : YAG laser. To obtain this profile, the FC was positioned at 14 cm away from target and 20° with respect to target normal.

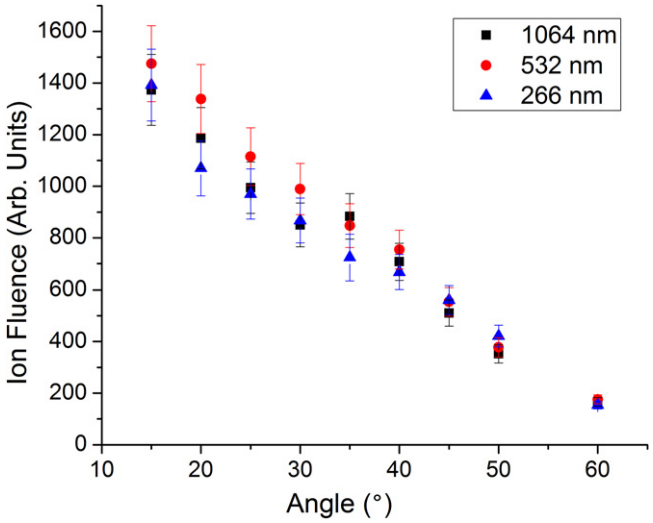

Figure 6. Angular dependence of ion fluence where the FC was positioned at 14 cm away from target on a rotatable mount.

QCM crystal under similar laser irradiation conditions for ω, 2ω and 4ω. From the figure, it is clear that all three Nd : YAG wavelengths' debris accumulations show a decreasing trend for increasing off-normal target angle, with 266 nm radiation consistently generating the most debris. The difference in debris generation as a function of wavelength, however, is not as pronounced as the difference between Nd : YAG and CO_2 elucidated in our previous work [11]. The clear forward bias of the Nd : YAG produced debris stands in contrast to that of the CO_2 LPP [11] and exists for both the second and fourth harmonics as well.

3.3. Ionic debris studies

Ionic emission was analyzed using the FC by positioning it 14 cm away from the target surface. Typical normalized kinetic energy profiles of Sn ions recorded at 20° with target normal for ω, 2ω and 4ω are given in figure 5. The kinetic energy profiles give a maximum probable ion kinetic energy of 1.2 keV, 1.3 keV and 1.4 keV for ω, 2ω and 4ω, respectively, representing a shift toward higher energy ions with decreasing wavelength. The ion kinetic energy profiles are found to be broader with decreasing wavelength of excitation.

Similar to QCM studies, for angular ion emission studies, the FC was fixed on a rotatable manipulator and was rotated on 5° intervals between 15° and 65°. Figure 6 shows the total ion flux recorded using the FC at various angles with respect to target normal. Clearly from figure 6, all Nd : YAG wavelengths exhibit forward bias in ionic debris. The linear decrease in debris for increasing off-normal angle exists for each wavelength, and each undergoes an order of magnitude drop in flux from 15° to 65°. The recorded ion flux and its variation with angle with respect to target normal showed similar characteristics regardless of the laser wavelength used.

4. Discussion

A comparison of atomic and ionic debris of Sn plasma generated by ω, 2ω and 4ω Nd : YAG radiation showed differences in EUV emission, angular variation in atomic deposition as well as kinetic profiles of ions. However, the visible emission spectra as well as angular ion flux showed similar features. It is well known that excitation wavelength, λ, plays a key role in the properties of the plasma generated by laser pulses. The laser excitation wavelength affects both laser–target (mass-ablation rate, penetration depth) and laser–plasma (absorption, reflection) coupling efficiencies, as well as optical properties of the plasma (opacity).

Typically, shorter wavelengths are preferred for LIBS and laser-ablation inductively coupled-plasma (LA-ICP-MS) elemental sensors [2]. Shorter wavelengths provide higher photon energies for bond breaking (molecules) and the ionization process. Moreover, the mass-ablation rate varies [22] with excitation wavelength as $\lambda^{-4/9}$. Hence laser–target coupling efficiency will be higher for shorter wavelength excitation. Though shorter wavelength excitation provides higher laser–target coupling and hence mass-ablation rate, previous studies showed that the fluence threshold for plasma formation is higher for 4ω compared to 2ω and ω [23]. This indicates the laser–plasma generation is ignited by inverse bremsstrahlung which is approximately proportional to λ^3.

The interaction of the laser beam with plasma is governed by two absorption mechanisms, inverse bremsstrahlung and photoionization, and both of these processes are wavelength dependent. The calculated ratio between absorption coefficients for different wavelengths ω, 2ω and 3ω showed approximately 9 : 2 : 1 [24]. Because of efficient reheating, plasmas generated by longer wavelength laser radiation possess higher temperatures. Hence, lower laser power densities are required for generating similar temperature plasmas with the use of longer wavelength excitation when keeping similar spot size. For example, for generating EUV-efficient Sn plasmas, the CO_2 10.6 μm laser requires

nearly one order lower power density compared to Nd : YAG 1.06 μm laser excitation [9]. The critical density of the plasma governs the location of the laser–plasma absorption or reheating. The critical density (n_c) of the plasmas, which scales with wavelength as λ^{-2}, generated by ω, 2ω, and 4ω, are 1×10^{21} cm^{-3}, 4×10^{21} cm^{-3} and 1.6×10^{22} cm^{-3}, respectively. Hence, shorter excitation wavelengths can penetrate higher density regions located closer to the target than longer wavelengths. By shortening the wavelength, the laser interacts closer to the target surface due to higher critical density of the plasma. However, higher density regions are relatively opaque and reabsorb a greater amount of emission than lower density outer regions. Previous reports also showed that, among the Nd : YAG harmonics, ω generates lower density and higher temperature plasmas [24] because of the one order reduction in critical density at ω compared to 4ω generated plasmas.

The recorded EUV spectra is found to be weaker with decreasing wavelength and plasma produced by 1064 nm showed maximum intensity, which is consistent with reported in-band conversion efficiencies [18]. Yamaura *et al* [18] reported that EUV emission exhibits angular dependence with excitation wavelength with shorter wavelength excitation (4ω) showing a sharper distribution ($\cos^{1.5}\theta$) compared to longer wavelength, ω, LPP ($\cos^{0.5}\theta$). Their EUV spectral studies also showed a wider and deeper spectral dip with decreasing excitation wavelength than the present experiments, indicating the 266 nm LPP is more opaque to plasma radiation. This could be due to the use of higher laser energy and larger spot size used in their studies [18]. Note that for better comparison we maintained similar spot size and power density for all wavelengths in the present investigations.

The UTA obtained from the shorter wavelength plasma (4ω) is found to be weaker in intensity and broader (figure 2). It should be mentioned that the optimum laser power density for producing the highest CE is different for different wavelengths and in the present scenario we used the optimum laser power density conditions for ω for all laser excitation wavelengths. Typically tin laser plasmas heated to 30 eV temperatures efficiently emit EUV radiation at 13.5 nm. Previous studies showed that higher laser power densities are necessary for obtaining optimum CEs using shorter wavelengths (2ω, 4ω) compared to ω [17]. Among the normalized spectra produced by fundamental and various harmonics of Nd : YAG laser, maintaining constant laser power density, the shortest wavelength fourth harmonic radiation provides the lowest CE and worst spectral purity. At constant laser power density, shorter wavelength radiation offers less efficient heating of the plasma due to a higher critical density. This results in a lower temperature, denser plasma, as the laser radiation is used to ablate more of the target surface rather than to reheat the already formed plasma [19, 25, 26]. Lower temperature plasmas contain ion distributions of lower average charge state than those from higher temperature plasmas [27]. It should be mentioned that highly charged ions (Sn^{9+}–Sn^{13+}) are responsible for emission in the in-band region [28] and lower charged ions contribute to the higher wavelength regions of the UTA, providing the broadening of the UTA seen on the higher wavelength side using shorter wavelength laser radiation. The spectral dips appearing around 13.5 nm suggest that the plasma is opaque to 13.5 nm radiation due to high plasma density resulting in strong self-absorption. These factors contribute to lower CE and worsened spectral purity at 13.5 nm observed from shorter wavelength radiation. The recorded EUV UTA spectra are found to be narrower with increasing wavelength due to higher plasma temperatures and lower populations of lower charged ions. This is consistent with our previous observation using the CO_2 LPP, where the narrowest UTA is produced [29]. Morris *et al* [21] recently reported that the UTA spectral profiles showed distinct variation with angle of detection. Note that the spectral measurement in the present experiment is made at 45° with respect to the target normal.

Although the OoB studies in the EUV spectral region around the UTA (8–18 nm) showed significant changes in the spectral features and intensities, the spectra recorded in the visible region displayed more or less similar features. The dominant mechanism for producing lower charged species, that is, those contributing VUV, UV, and visible emission, is collisional three-body recombination, the rate (R_c) of which is given by

$$R_c \alpha Z^3 \ln \sqrt{Z^2+1}\, T_e^{-9/2} n_e^2 n_i, \qquad (1)$$

where Z is the charge state, T_e is the electron temperature, and n_e and n_i are the electron and ion densities. Because of the higher critical density, the plasma generated by 4ω will be denser compared to longer wavelength produced plasma leading to enhanced three-body recombination and hence lower charged species. Our previous studies showed that 10.6 μm plasma generates more continuum radiation along with less spatial emission extension compared to 1.06 μm LPP which is susceptible to enhanced recombination [14].

The spectra given in figure 3 are recorded at a distance 1 mm from the target in a time-integrated manner and most of the emission is caused by excited neutrals and singly ionized lines. The rate equation for three-body recombination shows a n_e^2 dependence, therefore efficient recombination can be expected for shorter wavelength excited plasmas. The recombination process in an LPP depends both on the irradiation conditions and ambient environment. For plasma expansion in vacuum most of the recombination process is happening near the target surface where the density is maximum. Recent studies showed that the excitation wavelength also greatly influences the recombination processes [14, 30]. However, the recorded spectra did not show significant variation in the intensities. This could be due to collection of plasma emission at a very close distance (1 mm) from the target as well as temporal and spatial (along the line of sight) averaging. Spectral line intensities of Sn^+ were used for estimating temperature of the plasma using Boltzmann plot method. The Sn^+ lines considered for the Boltzmann plot were 684.4 nm ($6p^2P^o \rightarrow 6s^2S$), 645.4 nm ($6p^2P^o \rightarrow 6s^2S$), 558.9 nm ($4f^2F^o \rightarrow 5d^2D$), 556.2 nm ($6d^2D \rightarrow 6p^2P^o$) and 533.2 nm ($6d^2D \rightarrow 6p^2P^o$). The estimated electron temperature values obtained from the spectra are 1.1 ± 0.1 eV, 1.8 ± 0.3 eV and 1.7 ± 0.2 eV for ω, 2ω and 4ω respectively.

According to figure 4, the estimated deposition is higher for shorter wavelengths, especially at smaller angles. The scaling law for mass-ablation rate of a laser incident on a target is given by

$$\dot{m} = 3 \times 10^3 I^{5/9} A^{3/8} \lambda^{-4/9}, \quad (2)$$

where I is the laser intensity, λ is the wavelength of the laser and A is the atomic number [22]. Since similar laser intensities are used in the present experiment, the mass-ablation rate should follow a ratio of $1 : 1.36 : 1.86$ for ω, 2ω and 4ω, respectively. The recorded data using QCM showed consistently higher deposition for 4ω irrespective of angle used.

The ion kinetic energy profiles showed similar maximum probable peak energies for all laser wavelengths studied. The ion flux estimation showed similar results for all wavelengths used and both atomic and ionic debris showed distinct forward biasing toward the target normal. The angular distribution of ion flux showed rapid reduction with increasing angle from the target normal. The angular distribution of ions in an LPP are best approximated by a single charge dependent $\cos^n$ function where the value of n increases with the charge state and decreases with the atomic mass [31]. Recent studies by Morris *et al* [32] under similar irradiation conditions showed that the angular dependence of ion stages by summing the integrated ion signals of Sn^{1+}–Sn^{9+} followed a cosine fit. For an LPP, the ions of the highest ionization state dominate in the direction normal to the target, while their concentration falls sharply away from the normal direction, and excited neutrals display the most angular spread [31]. It should be noted that in the present experiments FCs were used for ion analysis and will not differentiate various ionization stages reaching the detector and the $\cos^n$ function will not accurately fit our data because of the limitations of the FC detection method. However, considering the angular-dependent behaviors of atomic and ionic flux, it is clear that the atoms have a more angular spread. This is due to increased recombination in the outer angular regions of the plume. The similarity in ion flux data obtained for various wavelengths studied can likely be attributed to two competing processes: a balancing of differing mass ablation and heating and ionization processes with different wavelengths. At shorter wavelengths more mass is expected to be ablated along with higher recombination, while at longer wavelengths less ablated mass with reduced recombination, coupled with increased heating of the plasma, is likely the cause of the similarities in ion flux. This is also supported by observation of higher atomic flux at shorter wavelength LPPs.

5. Conclusions

We compared angular emission features of atomic and ionic particles along with EUV and visible OoB emission features of Nd : YAG laser-produced plasmas at fundamental, second, and fourth harmonic wavelengths. For direct comparison we maintained similar laser intensities for all wavelengths studied. The EUV spectral studies showed highest in-band emission and spectral purity from the longer wavelength 1.06 μm radiation. The UTA recorded for shorter wavelength excitation showed broader spectra because of lower plasma temperature resulting in increased populations of lower ionic states that emit at higher wavelengths. The emission spectroscopy in the visible region revealed no great change in intensity between laser excitation wavelengths.

Ionic and atomic angular debris studies revealed a pronounced forward bias toward the target normal. Deposition studies using a quartz crystal microbalance showed the 266 nm wavelength to generate the most atomic particles, consistent with mass-ablation estimates. Though similar maximum ion kinetic energy was observed for all wavelengths investigated, the kinetic energy profiles are found to be broader with decreasing wavelength. This broadening is attributed to the enhanced three-body recombination in dense shorter wavelength plasmas. The angular dependence of ion flux showed similar trends as well as fluxes for all laser wavelengths. For an EUV source-development perspective, the 1064 nm Nd : YAG is the best option of the wavelengths studied in this report, owing to its higher 13.5 nm conversion efficiency and lower atomic debris.

Acknowledgments

This work is partially supported by Purdue University and SEMATECH Inc. The authors thank Matthew Fields for the initial experimental help.

References

[1] Banine V Y, Koshelev K N and Swinkels G H P M 2011 *J. Phys. D: Appl. Phys.* **44** 253001
[2] Singh J P and Thakur S N 2007 *Laser-Induced Breakdown Spectroscopy* (Amsterdam: Elsevier)
[3] Chrisey D B and Hubler G K 1994 *Pulsed Laser Deposition of Thin Films* (New York: Wiley)
[4] Al-Shboul K F, Harilal S S and Hassanein A 2011 *Appl. Phys. Lett.* **99** 131506
[5] Russo R E, Mao X L, Gonzalez J J and Mao S S 2002 *J. Anal. At. Spectrom.* **17** 1072–5
[6] Spitzer R C, Kauffman R L, Orzechowski T, Phillion D W and Cerjan C 1993 *J. Vac. Sci. Technol.* B **11** 2986–9
[7] Tanaka H, Matsumoto A, Akinaga K, Takahashi A and Okada T 2005 *Appl. Phys. Lett.* **87** 041503
[8] Harilal S S, Coons R W, Hough P and Hassanein A 2009 *Appl. Phys. Lett.* **95** 221501
[9] Harilal S S, Sizyuk T, Hassanein A, Campos D, Hough P and Sizyuk V 2011 *J. Appl. Phys.* **109** 063306
[10] Bollanti S, Di Lazzaro P, Flora F, Mezi L, Murra D and Torre A 2009 *Appl. Phys. B: Lasers Opt.* **96** 479–90
[11] Campos D, Harilal S S and Hassanein A 2010 *J. Appl. Phys.* **108** 113305
[12] Slaughter J M, *et al* 1994 *J. Appl. Phys.* **76** 2144–56
[13] Feigl T, Yulin S, Kuhlmann T and Kaiser N 2002 *Japan. J. Appl. Phys. 1* **41** 4082–5
[14] Campos D, Harilal S S and Hassanein A 2010 *Appl. Phys. Lett.* **96** 151501
[15] Hassanein A, Sizyuk V, Sizyuk T and Harilal S 2009 *J. Micro/Nanolithogr. MEMS MOEMS* **8** 041503
[16] Harilal S S, O'Shay B, Tao Y and Tillack M S 2006 *J. Phys. D: Appl. Phys.* **39** 484
[17] Miyamoto S, Shimoura A, Amano S, Fukugaki K, Kinugasa H, Inoue T and Mochizuki T 2005 *Appl. Phys. Lett.* **86** 261502

[18] Yamaura M *et al* 2005 *Appl. Phys. Lett.* **86** 181107
[19] White J, Dunne P, Hayden P, O'Reilly F and O'Sullivan G 2007 *Appl. Phys. Lett.* **90** 181502
[20] Ralchenko Y, Kramida A E and Reader J 2011 *NIST Atomic Spectra Database* NIST
[21] Morris O, O'Reilly F, Dunne P and Hayden P 2008 *Appl. Phys. Lett.* **92** 231503
[22] Burdt R A, Yuspeh S, Sequoia K L, Tao Y Z, Tillack M S and Najmabadi F 2009 *J. Appl. Phys.* **106** 033310
[23] Cabalin L M and Laserna J J 1998 *Spectrochim. Acta* B **53** 723–30
[24] Hoffman J, Moscicki T and Szymanski Z 2011 *Appl. Phys.* A **104** 815–9
[25] Shaikh N M, Hafeez S, Rashid B and Baig M A 2007 *Eur. Phys. J.* D **44** 371–9
[26] Rashid B, Hafeez S, Shaikh N M, Saleem M, Ali R and Baig M A 2007 *Int. J. Mod. Phys.* B **21** 2697–710
[27] Burdt R A, Tao Y Z, Tillack M S, Yuspeh S, Shaikh N M, Flaxer E and Najmabadi F 2010 *J. Appl. Phys.* **107** 043303
[28] White J, Cummings A, Dunne P, Hayden P and O'Sullivan G 2007 *J. Appl. Phys.* **101** 043301
[29] Freeman J R, Harilal S S and Hassanein A 2011 *J. Appl. Phys.* **110** 083303
[30] Shaikh N M, Tao Y, Burdt R A, Yuspeh S, Amin N and Tillack M S 2010 *J. Appl. Phys.* **108** 083109
[31] Thum-Jager A and Rohr K 1999 *J. Phys. D: Appl. Phys.* **32** 2827–31
[32] Morris O, O'Connor A, Sokell E and Dunne P 2010 *Plasma Sources Sci. Technol.* **19** 025007